J. Fluid Mech. (1981), *vol.* 108, *pp.* 133–146
Printed in Great Britain

An experimental investigation of the initial force of impact on a sphere striking a liquid surface

By M. MOGHISI AND P. T. SQUIRE
School of Physics, University of Bath, Bath BA2 7AY

(Received 11 June 1980)

Detailed experimental results are presented for the initial impact force on a sphere striking a horizontal liquid surface vertically at speeds in the range 1–3 m s^{-1}. Results are discussed in terms of an impact drag coefficient. Liquids having viscosities in the range 10^{-3}–10^{2} Pa s have been studied. For low viscosities the results have been compared with the theoretical calculations of Shiffman & Spencer. Good agreement has been found in most respects; in particular the impact force varies as the square root of the depth for depths less than a tenth of the radius. The impact drag coefficient has also been studied through the transition from inertia to viscosity-dominated conditions. The variation of the impact drag coefficient is presented as a function of Reynolds number, and its variation in the range $5 \times 10^{-2} < Re < 5 \times 10^{3}$ is shown to resemble that of a fully immersed sphere moving steadily in a homogeneous fluid.

1. Introduction

Studies of the impact of a solid sphere on a horizontal liquid surface have been mainly of two kinds: those which are concerned with the formation of the cavity and splash, and those which are concerned with the force of impact on the sphere. In the former category may be cited the work of Worthington (1908), Bell (1924), Richardson (1948), May (1951) and Abelson (1970, 1971). Gilbarg (1960) gives a review of cavity formation.

It is with the second aspect, the impact force on the sphere, that this study is concerned. The first reported measurements of this force were by Aoki (1928) and by Watanabe (1934); the latter used quartz transducers to display directly on an oscilloscope the force–time curves immediately following impact. Richardson (1948) and May & Woodhull (1948, 1950) derived the force from position–time curves obtained from high-speed cinephotographs. They were concerned with a later stage of entry, when the sphere was fully submerged and accompanied by a well-formed cavity. The initial shock of impact may have important structural effects on the impinging body. These have been reviewed by Kornhauser (1964). A further effect which may occur following oblique impact is ricochet (Johnson & Daneshi 1978).

Very few theoretical calculations have been made of the impact force; this is not surprising in view of the immense complexity of the hydrodynamics of the process. The most ambitious attempt relevant to this study was by Shiffman & Spencer (1945*a*, *b*). In view of the obscurity of their work a summary is given in § 2. Hu (1958) also discussed the problem. The case of oblique entry was treated by Trilling (1950).

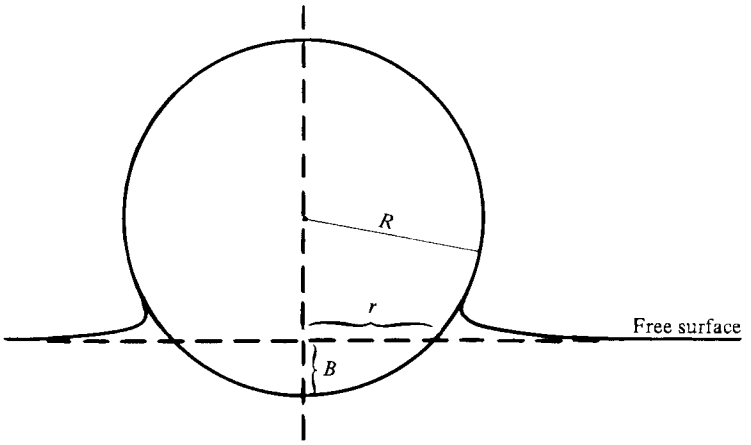

FIGURE 1. Geometry of sphere entry.

Related studies of the simpler but still formidable problem of wedge entry have been reviewed by Hughes (1972).

The objects of this study are twofold: first to test the Shiffman–Spencer theory for the impact force during the very early stage of entry; and secondly to present results on the force–time relationship for low-Reynolds-number conditions ($Re < 1$), which have not been studied before.

Results are most conveniently presented and discussed in terms of a dimensionless 'impact drag coefficient' C_d, defined by analogy with the conventional drag coefficient for a body in a homogeneous fluid. Accordingly we write

$$F = \tfrac{1}{2}C_d A\rho v^2, \tag{1}$$

where F is the impact force, A is the cross-sectional area, ρ is the fluid density and v is the velocity of the body. It is important to remember that C_d depends on the depth of immersion in addition to any dependence on Reynolds number.

2. Summary of Schiffman–Spencer theory

The following summary of the theory of Shiffman & Spencer (1945*a*, *b*) is given because the original reports are not widely available.

Consider a three-dimensional half-space filled with liquid of density ρ, with a horizontal free surface. Initially at rest, it is struck by a sphere, radius R, moving with velocity v vertically downwards. Figure 1 shows the situation a short time after impact. The tip of the sphere has penetrated a distance B below the free surface. The liquid in the vicinity of the impact has been set in motion and a meniscus has partly formed.

After the sphere has penetrated some distance further the liquid may separate from the sphere, leading to cavity formation (Worthington 1908). However, the stage of the impact under consideration here is before separation has commenced; the depth B is less than half the radius R.

The upward impact force F at any instant t may be expressed in terms of the virtual mass M of the liquid through the relation

$$F = d(Mv)/dt.$$

If M_0 be the mass of the sphere, neglecting the gravitational force we have also

$$-F = d(M_0 v)/dt, \tag{2}$$

and therefore $$(d/dt)\,[(M+M_0)\,v] = 0.$$

After integration this becomes

$$(M+M_0)\,v = M_0 v_0,$$

where v_0 is the velocity of the sphere at impact. It follows that

$$v = \frac{v_0}{1+M/M_0}. \tag{3}$$

Now $$v = dB/dt.$$

Therefore, differentiating (3) and using (2), we find that

$$F = \frac{(dM/dB)\,v_0^2}{(1+M/M_0)^3}. \tag{4}$$

Let $$m = M/(\tfrac{1}{2}\pi\rho R^3)$$

and $$b = B/R. \tag{5}$$

Then from (1), (4) it follows that

$$C_d = \frac{dm/db}{(1+M/M_0)^3}.$$

One further dimensionless parameter is used, to express the effective specific gravity of the sphere relative to the liquid, namely

$$\sigma = M_0/(\tfrac{4}{3}\pi R^3\rho). \tag{6}$$

Thus we may write $$C_d = \frac{dm/db}{(1+3m/8\sigma)^3}. \tag{7}$$

This shows that if the mass of the sphere is large compared to the mass of the liquid displaced the impact drag coefficient is to a good approximation equal to (dm/db).

Shiffman & Spencer (1945*a*, *b*) calculated $m(b)$ by setting up an approximate velocity potential, employing the method of multi-valued dipoles and images. Further details of this method may be found in Shiffman & Spencer (1947). Corrections were made for the rise of the meniscus ('wetting factor') and the rise of the free surface ('free surface correction').

The final results are shown graphically in figure 2. These show that the impact drag coefficient, and hence the impact force, rise rapidly to a maximum when the depth of penetration is between a tenth and a fifth of the radius ($0{\cdot}1 < b < 0{\cdot}2$). Thereafter it declines more gradually towards a value of between 0·25 and 0·3, when the cavity is fully formed (May & Woodhull 1948, 1950). The precise shape depends on the specific gravity σ. Values of σ may be made arbitrarily large by loading the sphere so that its total mass M_0 is much greater than the displaced mass of water ($\frac{4}{3}\pi R^3\rho$). Watanabe (1934) used a truncated sphere of large radius (15 cm) so that σ was much less than 1. This makes the comparison of experimental results with (7) complicated since both (dm/db) and m are significant. In this study σ was made sufficiently large for the term involving m in the denominator of (7) to be neglected.

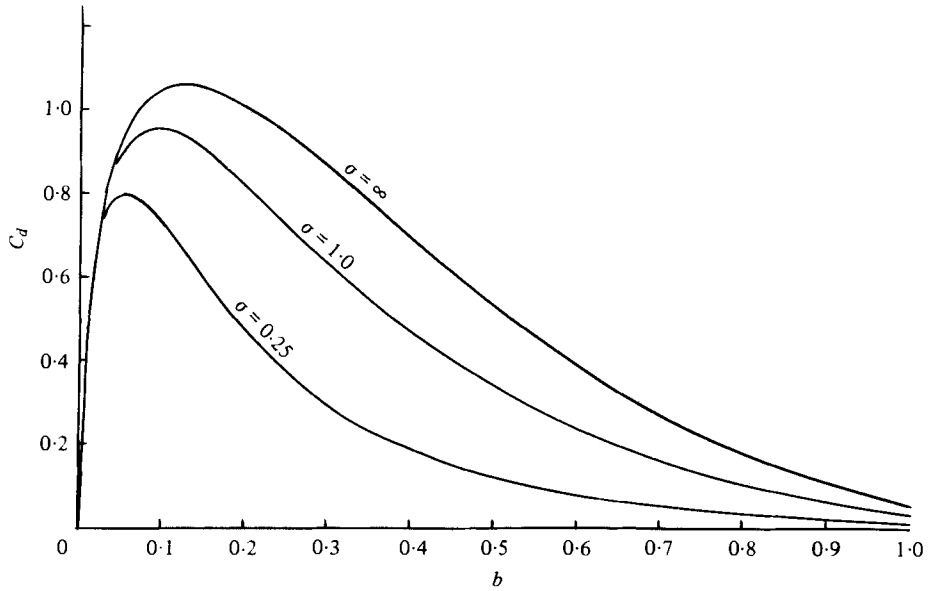

FIGURE 2. Theoretical value of impact drag coefficient C_d against normalized depth of immersion b (after Shiffman & Spencer).

The detailed behaviour of C_d for $b < 0{\cdot}1$ is not clearly shown in figure 2. Shiffman & Spencer give an explicit relationship for this region,

$$C_d = a_1 b^{\frac{1}{2}} - a_2 b, \tag{8}$$

where $a_1 = 5{\cdot}40.$

(An error in the original paper leads to a value of 6·62.) The coefficient a_2 is not accurately given by the theory. For sufficiently small values of b, equation (8) predicts that C_d should vary as $b^{\frac{1}{2}}$, so that on log/log scales a graph of C_d against b should be linear with a slope of $\frac{1}{2}$. An experimental test of this prediction and an experimental determination of the coefficients a_1, a_2 is one of the main objects of this study.

3. Apparatus used for impact-force measurement

3.1. *General arrangement*

Figure 3 shows the general mechanical arrangement of the apparatus. The transducer assembly fell under controlled conditions onto the surface of the liquid, which was contained in a temperature-controlled oil bath.

3.2. *Transducer assembly*

The body used for studying the impact force was a steel hemisphere cut from a steel ball 25 mm in diameter. This formed the front section of a piezoelectric transducer assembly (figure 4). The active element was a modified lead zirconate titanate (PZT) disk 25 mm in diameter and 2 mm thick (Mullard PXE 5 type MB1068). The main body of the transducer consisted of a copper cylinder 38 mm in diameter and 62 mm long. The total mass was 0·665 kg, giving $\sigma = 81$ in (6) and (7).

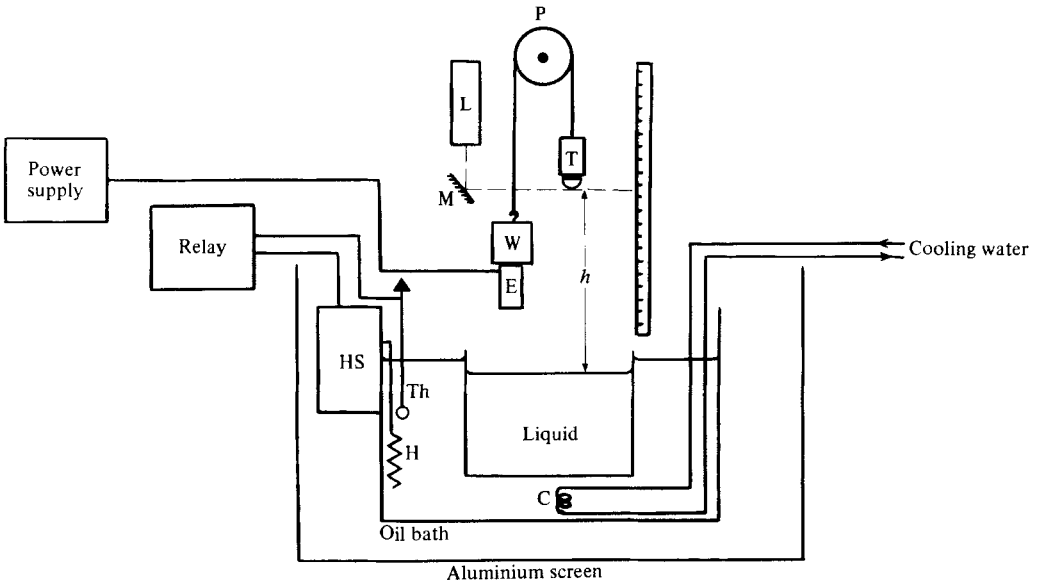

FIGURE 3. General arrangement of apparatus: C, cooling coil; E, electromagnet; H, heater; HS, heater supply; L, laser; M, mirror; P, pulley; T, transducer; Th, thermometer; W, counterweight.

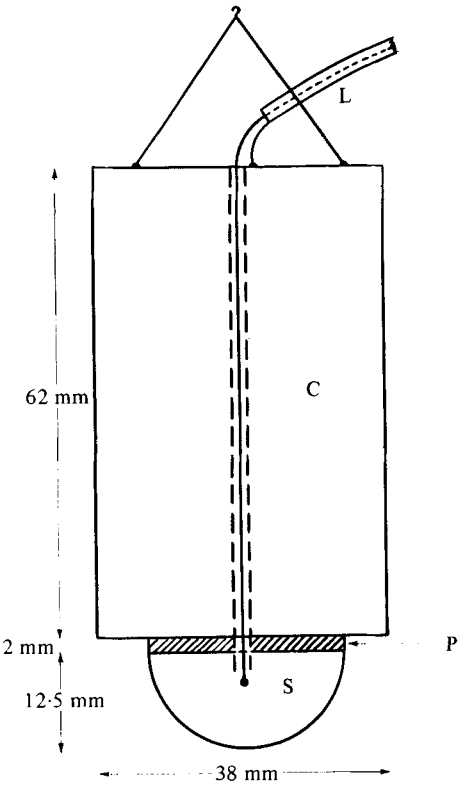

FIGURE 4. Transducer assembly. C, copper cylinder; L, coaxial lead; P, piezoelectric disk; S, steel hemisphere.

Electrical contact with the front face of the PZT disk was made through an axial hole. The capacitance of the transducer and cable was measured as 3·9 nF at frequencies well below fundamental resonance ($\sim$ 35 kHz).

3.3. *Control of the impact velocity*

The transducer assembly was suspended by means of a thread, which ran over a pulley to a counterweight. The purpose of this was to reduce the acceleration of the falling body to enable the impact velocity to be controlled in the range 0·5–3 m s^{-1} by releasing it from heights h in the range 20–50 cm. The height h was set precisely with the aid of a laser beam and mirror scale. The motion was arrested before the top of the hemisphere had penetrated below the free surface, in order to avoid excessive take-up of liquid by the transducer assembly. Thus the maximum normalized depth which could be studied was $b = 1$. In practice the limit was lower than this because the rising meniscus shorted out the transducer when b reached between 0·5 and 1.

The impact velocity was calculated using the relation

$$v_0 = (2ah)^{\frac{1}{2}},$$

where the acceleration a could be varied from 1 m s^{-2} to 6 m s^{-2} by adjusting the counterweight. Strictly speaking allowance should be made for the change in impact velocity during entry. However, in all the measurements reported here the velocity remained effectively constant, the maximum change being well below 1 % even for the most viscous liquid (Moghisi 1979).

3.4. *Liquids used for the impact-force measurements*

The liquids were contained in a glass tank 20 cm high, with a base 16 × 10 cm. The walls were 5 mm thick. The depth of liquid was about 15 cm, requiring a volume of some 2·4 litres. The range of viscosity of the liquids used was from 10^{-3} to $\sim 10^2$ Pa s. This was achieved by the use of mixtures of water and Golden Syrup, and by varying the temperature between 15 °C and 30 °C. The viscosity of each liquid used was measured at the appropriate temperature using either an Ostwald-type U-tube viscometer or a falling-sphere viscometer, in accordance with BS 188. The densities were also measured.

3.5. *Signal detection and recording*

The electrical circuit is shown in figure 5. The transducer output was connected to a transient recorder (Datalab DL 905). The decade capacitor unit was connected across the input terminals in order to increase the time constant of the input circuit. For all the measurements reported here the total input capacitance was 50 nF and the input resistance was 1 MΩ, giving a time constant of 50 ms. Since the longest time involved in the measurement of impact force was about 1 ms any distortion of the signal due to leakage across the input circuit has been neglected. The transient recorder output was monitored with an oscilloscope and displayed on a chart recorder for analysis.

3.6. *System calibration*

The chart recorder trace is a linearly scaled representation of the force–time curve. In order to derive absolute values of force and time from the trace it was necessary to know the calibration factors of the x and y scales. These may be defined through the relations

$$x = Xt, \quad y = YF,$$

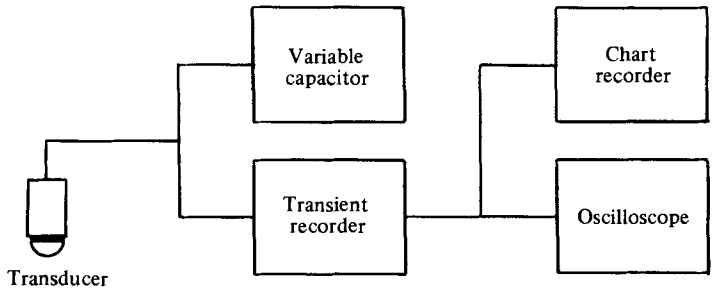

FIGURE 5. Electrical circuit.

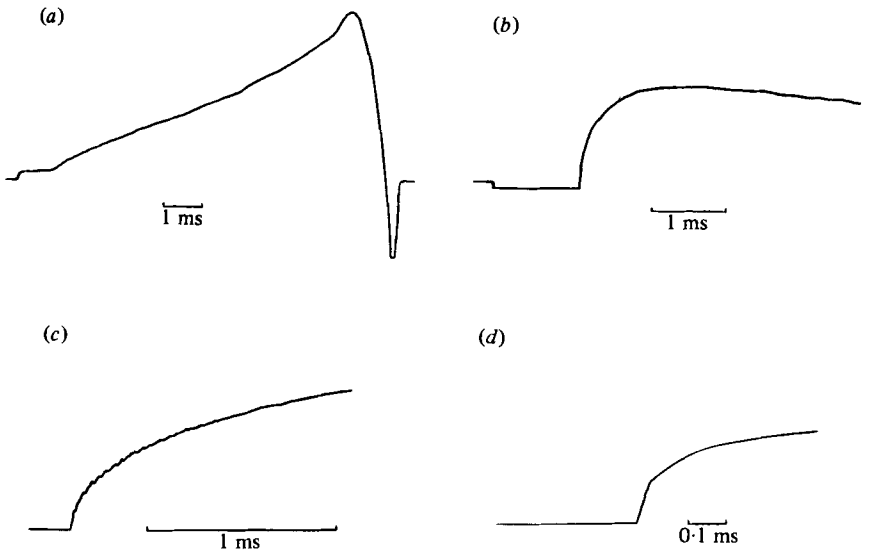

FIGURE 6. Typical force-time curves. The force scale (vertical) is in arbitrary units and is not the same in each case.

	(*a*)	(*b*)	(*c*)	(*d*)
Impact velocity (m s^{-1})	0·73	1·87	1·39	2·43
Viscosity (Pa s)	0·001	0·008	1·1	0·001

where X is the factor relating chart length to real time and Y is the factor relating chart width to force; X may be easily and accurately derived from the transient recorder data. The crystal-controlled timebase is accurately known. The length of chart corresponding to this is clearly recognizable because a sharp step in the output occurs at the start and finish of the plot cycle. Thus the chart length corresponding to the timebase may be measured directly from the chart. Knowledge of the plot time and chart speed are not required.

Determination of the force calibration factor Y is less straightforward. An absolute calibration method was devised, based on the impulse produced by a swinging pendulum. The method has been described in detail elsewhere (Moghisi & Squire 1980).

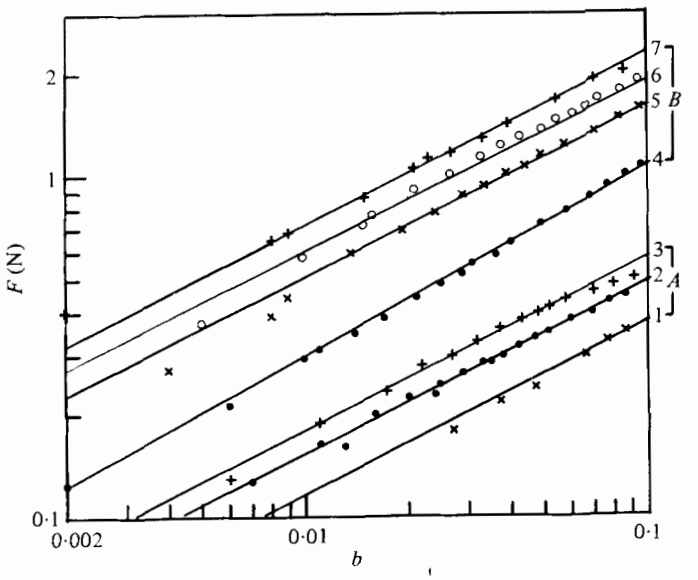

FIGURE 7. Impact force F against normalized depth b with impact velocity as parameter. Curves 1–3 (A) are for viscosity of 0·008 Pa s; curves 4–7 (B) are for viscosity of 20 Pa s. Impact velocities in m s^{-1} as follows: (1) 0·97, (2) 1·10, (3) 1·30, (4) 0·95, (5) 1·26, (6) 1·41, (7) 1·56. Solid lines are visual interpolations drawn for guidance.

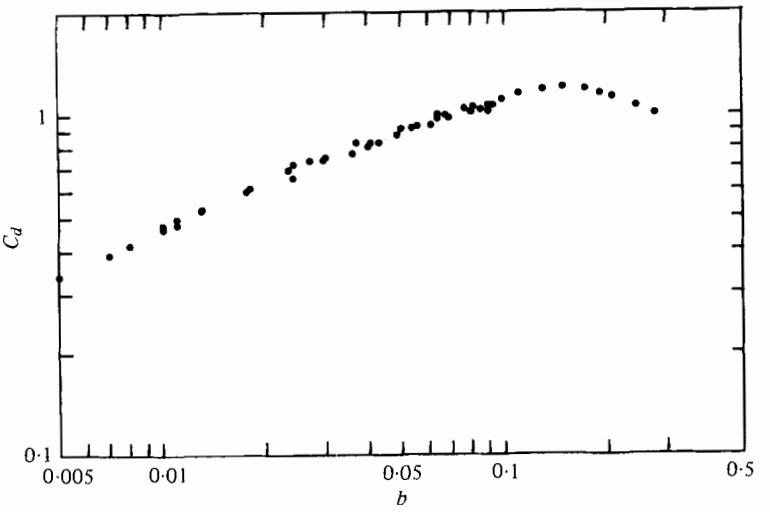

FIGURE 8. Impact drag coefficient C_d against normalized depth b for impact velocities in the range 1–3 m s^{-1} (water).

4. Results

4.1. *Typical force–time curves*

Some selected force–time curves are shown in figures 6(a)–(d). These have been chosen merely to illustrate the variety of curves that may be obtained as the impact velocity and viscosity are varied. Figure 6(a) shows that for sufficiently low impact velocities in water (< 1 m s^{-1}) the force rises without a marked sudden onset. Figure

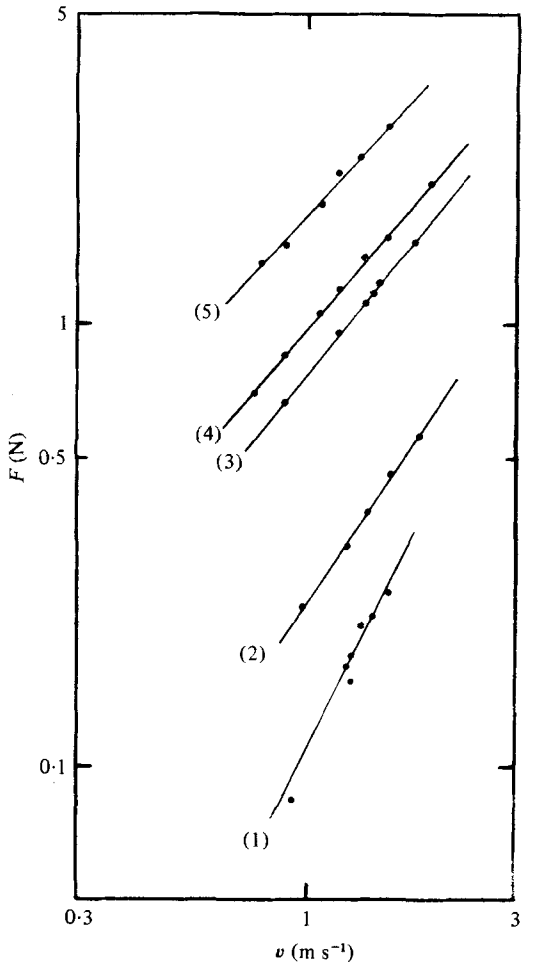

FIGURE 9. Impact force F against impact velocity v at a normalized depth $b = 0{\cdot}01$, with viscosity as parameter. Viscosity values in Pa s: (1) 0·001, (2) 1·1, (3) 22·5, (4) 26, (5) 82. Slopes of log plots are: (1) 1·97, (2) 1·47, (3) 1·24, (4) 1·16, (5) 1·09.

6(*b*) shows the behaviour typical of impact velocities between 1 and 3 m s^{-1}; there is an initial sudden rise followed by a more gradual rise to the maximum, after which the force decreases much more gradually. The maximum force occurs very soon after entry: in this case some 1·5 ms after initial impact, at which time the tip of the sphere has penetrated a distance equal to about one fifth the radius ($b \sim 0{\cdot}2$). This is consistent with the general behaviour predicted by the Shiffman–Spencer model and shown in figure 2.

In figure 6(*c*) the time base is shorter and some small oscillations may be seen on the rising edge. These are due to ringing of the transducer and may be removed by filtering if required. This is shown in figure 6(*d*), which was obtained with a low-pass filter inserted between the transducer and transient recorder (Barr and Stroud type EF3-06, 30 kHz cut-off, 24 dB per octave). Figures 6(*c*) and (*d*) are typical of the force–time curves used to derive the impact drag coefficient.

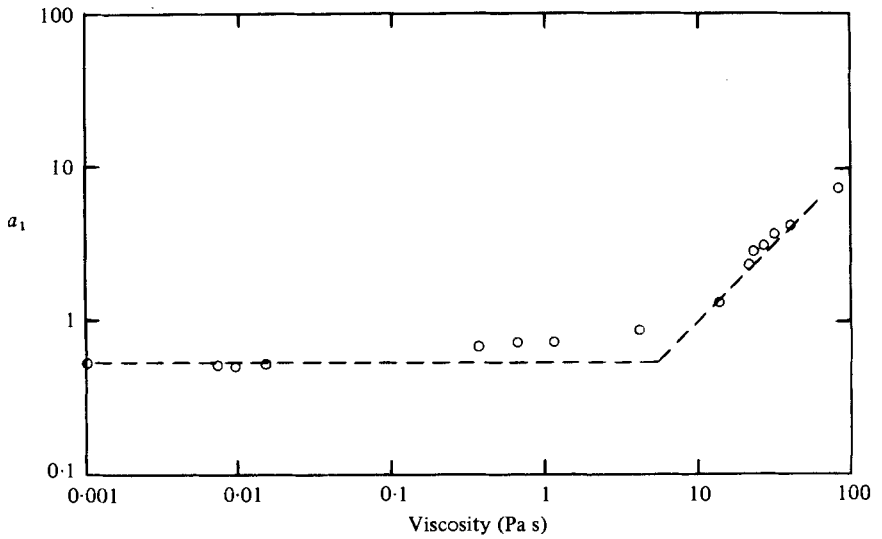

FIGURE 10. Coefficient a_1, used in equation (8) to calculate impact drag coefficient, against viscosity. The broken lines are drawn for guidance.

4.2. *Impact force as a function of depth and velocity*

According to (1) and (8) the initial impact force should vary as $b^{\frac{1}{2}}$, where the normalized depth b is defined in (5). Thus log/log plots of impact force F against b should be linear for $b \ll 1$. Examples of such plots are shown in figure 7; there it will be noted that, except for the lowest velocity of impact with water, the results conform closely to the $b^{\frac{1}{2}}$ dependence for $b \lesssim 0{\cdot}1$. Results for water over a wider range of depth are shown in figure 8 in terms of the impact drag coefficient C_d defined in (1).

The Shiffman–Spencer theory predicts that C_d is independent of velocity. According to (1) it follows that F should vary as v^2. Graphs of F against v on log/log scales are shown in figure 9. These were derived from graphs like those shown in figure 7 by drawing the ordinate $b = 0{\cdot}01$ and plotting the points of intersection with the families of lines for each value of viscosity. The choice of $b = 0{\cdot}01$ is arbitrary; any value in the range 0·005–0·1 would be appropriate. Since the force varies as $b^{\frac{1}{2}}$ (figure 7) the choice of $b = 0{\cdot}01$ makes scaling convenient.

The most significant point to note in figure 9 is the change in the velocity dependence of force as the viscosity increases. For low viscosity $F \propto v^2$, whereas for high viscosity $F \propto v$. The Shiffman–Spencer theory is only applicable in the inviscid limit, and is therefore consistent with these results.

4.3. *Variation of impact drag coefficient with viscosity*

The change in the velocity dependence of drag force with viscosity has already been indicated in figure 9. Figure 7 shows that over the whole range of viscosity studied the impact force varies as $b^{\frac{1}{2}}$ for $b \ll 1$. It is possible therefore to describe the initial impact force by (1) taking for C_d the first term in (8); i.e.

$$C_d = a_1 b^{\frac{1}{2}} \quad (b \ll 1).$$

Figure 10 shows the results calculated on this basis; the coefficient a_1 is plotted against viscosity.

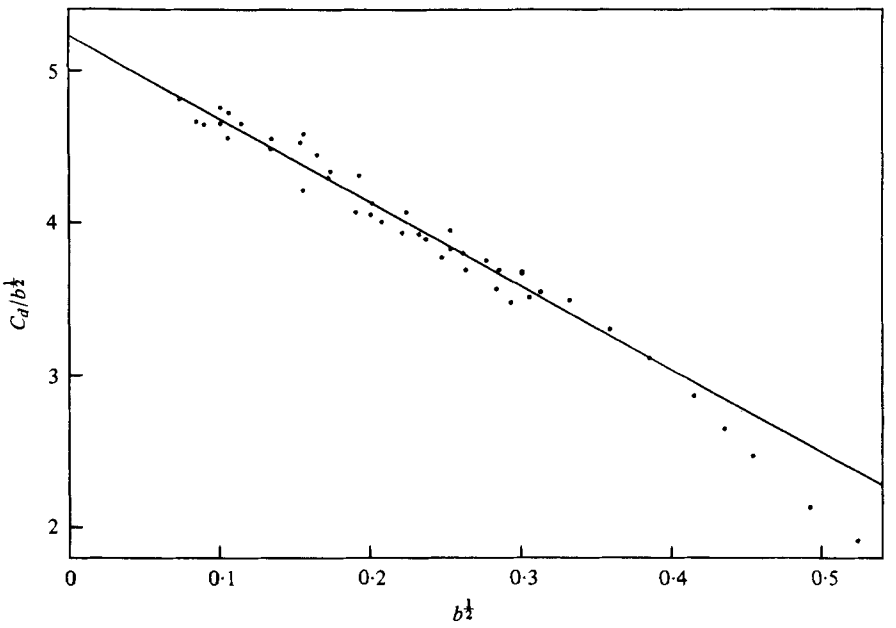

FIGURE 11. $C_d/b^{\frac{1}{2}}$ against $b^{\frac{1}{2}}$ for water, with impact velocities in the range 1·2–2·8 m s^{-1}. The linearity is a test of (9). The least-squares straight line is shown (ignoring four points at lower right). The intercept is a_1 and the slope is $-a_2$.

5. Analysis and discussion

5.1. *Impact drag coefficient as a function of depth*

The first objective of this work has been to test the Shiffman–Spencer theory, in particular the relationship (8) between impact drag coefficient C_d and normalized depth of immersion b:

$$C_d = a_1 b^{\frac{1}{2}} - a_2 b.$$

Strong support for the $b^{\frac{1}{2}}$ term is given by figures 7 and 8. The data for water in figures 7 and 8 have been analysed in two ways to extract values of the coefficients a_1 and a_2, and to test the functionality.

First it has been assumed that (8) is of the correct form, so that after division by $b^{\frac{1}{2}}$ it may be written

$$C_d/b^{\frac{1}{2}} = a_1 - a_2 b^{\frac{1}{2}}. \tag{9}$$

Thus a graph of $C_d/b^{\frac{1}{2}}$ against $b^{\frac{1}{2}}$ should be linear, with slope $(-a_2)$ and intercept a_1. Figure 11 shows the resulting plot over the range $0{\cdot}005 < b < 0{\cdot}275$, so it includes data up to and slightly beyond the peak in C_d (figure 8). Apart from the four points at the lower right ($b > 0{\cdot}18$) the data may be reasonably fitted by a straight line. The least-squares fit to the remaining 42 points (regressing y on x) gives

$$a_1 = 5{\cdot}22 \pm 0{\cdot}10, \quad a_2 = 5{\cdot}49 \pm 0{\cdot}43,$$

with 99 % confidence. This line is shown in figure 11. It is clear that for $b > 0{\cdot}18$ higher-order terms need to be added to (9).

In the second method of analysis it is not assumed that the powers of b in (8) are

necessarily $\frac{1}{2}$ and 1; instead they are treated as adjustable parameters p and q. We write

$$C_d = a_1 b^p - a_2 b^q. \tag{10}$$

This is now a nonlinear regression problem. It has been solved iteratively, using initial values of $a_1 = 5{\cdot}22$ and $p = 0{\cdot}5$ as obtained previously. The results are

$$a_1 = 5{\cdot}28 \pm 0{\cdot}03, \quad a_2 = 5{\cdot}71 \pm 0{\cdot}16,$$

$$p = 0{\cdot}503 \pm 0{\cdot}008, \quad q = 1{\cdot}01 \pm 0{\cdot}05,$$

with 99 % confidence. The powers p and q do not differ significantly from $\frac{1}{2}$ and 1 respectively, and the values of a_1, a_2 obtained by the two methods of analysis agree within their respective limits. We may reasonably conclude that (8) gives an adequate description of the impact drag coefficient for $b < 0{\cdot}18$, which includes the whole of the rising portion of the $C_d(b)$ curve.

The value of a_1 calculated here is very close to the value of 5·40 calculated theoretically by Shiffman & Spencer (see § 2), perhaps fortuitously so in view of the difficulty in calculating the wetting factor.

It should be pointed out, however, that, if these values of a_1 and a_2 are used to calculate the value of b for which C_d is a maximum, the result is not in close agreement with the experimentally observed value. The value of a_2 differs substantially from the value of 22 given by Shiffman & Spencer. However, that value was derived from less precise data of Watanabe (1934).

5.2. *Impact drag coefficient as a function of Reynolds number*

It is rather remarkable that the $b^{\frac{1}{2}}$ dependence of C_d observed for low viscosity appears to be maintained over the whole range of viscosity. This may be seen in figure 7. On the other hand, figure 9 shows that the velocity dependence of impact force varies with viscosity. This is suggestive of the drag behaviour of a sphere moving at constant velocity in a homogeneous fluid (e.g. Massey 1979). In that case, at a low Reynolds number Stokes' law gives

$$F = 6\pi R\eta v,$$

where η is the liquid viscosity. Alternatively, if the more general form (1) for the drag force be retained, the drag coefficient C_D must be written as

$$C_D = 24/Re,$$

where

$$Re = d\rho v/\eta, \tag{11}$$

the Reynolds number; d is a characteristic length of the body, in the case of a fully immersed sphere its diameter. However, for a partly immersed sphere the full diameter is not an appropriate parameter because the liquid 'does not know' any dimension of the sphere above the surface. It is more realistic to take the diameter of the circle of contact (ignoring wetting), shown in figure 1. This is given by

$$d = 2R(2b)^{\frac{1}{2}} \quad (b \ll 1);$$

for example, for $b = 0{\cdot}01$ and $2R = 25$ mm, $d = 3{\cdot}54$ mm. Substituting this value of d into (11), with $v = 1$ m s^{-1} and values of η and ρ for water, we find

$$Re \sim 3{\cdot}5 \times 10^3.$$

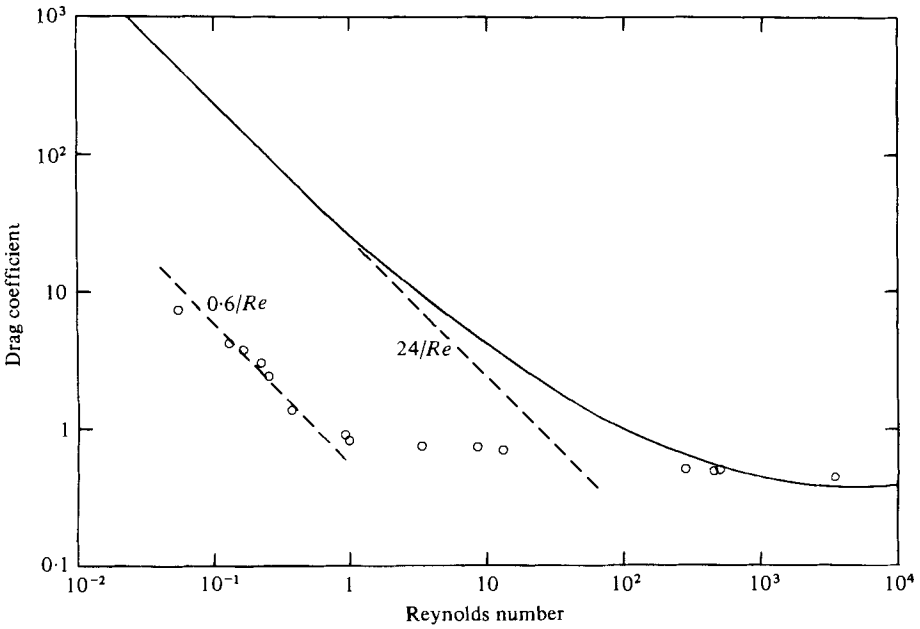

FIGURE 12. Impact drag coefficient C_d against Reynolds number Re at a normalized depth $b = 0{\cdot}01$. Experimental points from this study are shown as open circles. The continuous line shows the drag coefficient of a sphere in a homogeneous fluid. At low Re both drag coefficients vary as $1/Re$.

The results are shown in figure 12, in which the impact drag coefficient has been plotted against Reynolds number for $b = 0{\cdot}01$, together with the corresponding curve for the fully immersed sphere (Massey 1979). It should be borne in mind in comparing the drag behaviour for the two cases that C_d and Re both depend on b, and so by choosing different values of b the data may be shifted horizontally and vertically to some extent.

6. Conclusions

The impact drag force on a sphere striking a liquid surface has been measured at depths up to about a quarter of the radius ($0 < b < 0{\cdot}25$) and for impact velocities between 1 and 3 m s^{-1}. For $b < 0{\cdot}18$ the force may be adequately described by an impact drag coefficient C_d whose value is given by

$$C_d = a_1 b^{\frac{1}{2}} - a_2 b,$$

in accordance with calculations by Shiffman & Spencer. The value of a_1 found for water was $5{\cdot}22 \pm 0{\cdot}10$, compared with the calculated value of 5·40. The value of a_2 found for water was $5{\cdot}49 \pm 0{\cdot}43$, compared with a value of 22 deduced by Shiffman & Spencer from earlier measurements by Watanabe.

The impact drag coefficient has also been studied over a wide range of viscosity. It has been found that, for $b \ll 1$, $C_d \propto b^{\frac{1}{2}}$, and the dependence of C_d on Reynolds number in the range $0{\cdot}05 < Re < 5 \times 10^3$ resembles that of a sphere in a homogeneous fluid.

Most of this work was carried out as part of the programme for the M.Sc. degree of the University of Bath awarded to M. Moghisi. The authors wish to thank Professor G. A. Saunders, Head of the School of Physics, for the facilities afforded. Thanks are also due to Bob Draper, Eddie and Wendy Lambson of the School of Physics and Peter Wakeford of the School of Materials Science for technical assistance and advice.

REFERENCES

ABELSON, H. I. 1970 Pressure measurements in the water-entry cavity. *J. Fluid Mech.* **44**, 129–144.

ABELSON, H. I. 1971 A prediction of water-entry cavity shape. *Trans. A.S.M.E.* D, *J. Basic Engng* **93**, 501–504.

AOKI, T. 1928 *J. Soc. Ord. and Expl.* **21**, 249.

BELL, G. E. 1924 On the impact of a solid sphere with a fluid surface. *Phil. Mag.* **48**, 753–764.

GILBARG, D. 1960 Jets and cavities. In *Encyclopaedia of Physics* vol. 9 (ed. Flügge). Springer.

HU, P. N. 1958 On the water entry problem. Sc.D. thesis, Stevens Institute of Technology.

HUGHES, O. F. 1972 Solution of the wedge entry problem by numerical conformal mapping. *J. Fluid Mech.* **56**, 173–192.

JOHNSON, W. & DANESHI, G. H. 1978 Results for the single ricochet of spherical-ended projectiles off sand and clay at up to 400 m/sec. *I.U.T.A.M. Symp.* (1977) *on the High-Velocity Deformation of Solids*, pp. 317–344. Springer.

KORNHAUSER, M. 1964 *Structural Effects of Impact.* Baltimore: Spartan.

MASSEY, B. S. 1979 *Mechanics of Fluids.* Rheinhold.

MAY, A. 1951 The effect of surface conditions of a sphere on its water-entry cavity. *J. Appl. Phys.* **22**, 1219–1222.

MAY, A. & WOODHULL, J. C. 1948 Drag coefficients of steel spheres entering water vertically. *J. Appl. Phys.* **19**, 1109–1121.

MAY, A. & WOODHULL, J. C. 1950 The virtual mass of a sphere entering water vertically. *J. Appl. Phys.* **21**, 1285–1289.

MOGHISI, M. 1979 An experimental investigation of the force of impact on a sphere striking a liquid surface. M.Sc. thesis, University of Bath.

MOGHISI, M. & SQUIRE, P. T. 1980 An absolute impulsive method for the calibration of force transducers. *J. Phys.* E (To be published).

RICHARDSON, E. G. 1948 The impact of a solid on a liquid surface. *Proc. Phys. Soc.* **61**, 352–367.

SHIFFMAN, M. & SPENCER, D. C. 1945*a*, *b* The force of impact on a sphere striking a water surface. AMP *Rep.* 42, 1R, 42. 2R. AMG-NYU Nos. 105, 133.

SHIFFMAN, M. & SPENCER, D. C. 1947 The flow of an ideal incompressible fluid about a lens. *Quart. Appl. Math.* **5**, 270–288.

TRILLING, L. 1950 The impact of a body on a water surface at an arbitrary angle. *J. Appl. Phys.* **21**, 161–170.

WATANABE, S. 1934 Resistance of impact on water surface. Part V – sphere. *Inst. Phys. Chem. Res. Sci. Papers* **484**, 202–208.

WORTHINGTON, A. M. 1908 *A Study of Splashes.* Longmans. (Reprinted 1963, Macmillan.)